THE JOURNAL OF BIOLOGICAL CHEMISTRY VOL. 281, NO. 13, pp. 8907–8916, March 31, 2006

Structural and Functional Characterization of PseC, an Aminotransferase Involved in the Biosynthesis of Pseudaminic Acid, an Essential Flagellar Modification in *Helicobacter pylori*[*]

Received for publication, December 5, 2005, and in revised form, January 12, 2006 Published, JBC Papers in Press, January 18, 2006, DOI 10.1074/jbc.M512987200

Ian C. Schoenhofen[‡], Vladimir V. Lunin[§], Jean-Philippe Julien[¶], Yunge Li[§], Eunice Ajamian[¶], Allan Matte[§], Miroslaw Cygler[§¶], Jean-Robert Brisson[‡], Annie Aubry[‡], Susan M. Logan[‡], Smita Bhatia[‡], Warren W. Wakarchuk[‡], and N. Martin Young[‡1]

From the [‡]Institute for Biological Sciences, National Research Council, Ottawa, Ontario K1A 0R6, the [§]Biotechnology Research Institute, National Research Council, Montreal, Quebec H4P 2R2, and the [¶]Department of Biochemistry, McGill University, Montreal, Quebec H3G 1Y6, Canada

Helicobacter pylori **flagellin is heavily glycosylated with the novel sialic acid-like nonulosonate, pseudaminic acid (Pse). The glycosylation process is essential for assembly of functional flagellar filaments and consequent bacterial motility. Because motility is a key virulence factor for this and other important pathogens, the Pse biosynthetic pathway offers potential for novel therapeutic targets. From recent NMR analyses, we determined that the conversion of UDP-α-D-GlcNAc to the central intermediate in the pathway, UDP-4-amino-4,6-dideoxy-β-L-AltNAc, proceeds by formation of UDP-2-acetamido-2,6-dideoxy-β-L-*arabino*-4-hexulose by the dehydratase/epimerase PseB (HP0840) followed with amino transfer by the aminotransferase, PseC (HP0366). The central role of PseC in the *H. pylori* Pse biosynthetic pathway prompted us to determine crystal structures of the native protein, its complexes with pyridoxal phosphate alone and in combination with the UDP-4-amino-4,6-dideoxy-β-L-AltNAc product, the latter being converted to the external aldimine form in the active site of the enzyme. In the binding site, the AltNAc sugar ring adopts a $^4C_1$ chair conformation, which is different from the predominant $^1C_4$ form found in solution. The enzyme forms a homodimer where each monomer contributes to the active site, and these structures have permitted the identification of key residues involved in stabilization, and possibly catalysis, of the β-L-*arabino* intermediate during the amino transfer reaction. The essential role of Lys^{183} in the catalytic event was confirmed by site-directed mutagenesis. This work presents for the first time a nucleotide-sugar aminotransferase co-crystallized with its natural ligand, and, in conjunction with the recent functional characterization of this enzyme, these results will assist in elucidating the aminotransferase reaction mechanism within the Pse biosynthetic pathway.**

Flagellar glycosylation is common among a number of bacterial pathogens and has been implicated in immune avoidance, host/pathogen interactions, as well as in flagellar function and assembly (1–4). In *Helicobacter pylori* and *Campylobacter jejuni*, glycosylation of flagellin is required for the assembly of functional flagella, making its biosynthetic pathway a possible target for therapeutic intervention. Of particular interest are enzymes playing key roles in these pathways. Recently, mass spectrometry analysis of the *H. pylori* flagellar filament demonstrated that each flagellin monomer is modified with a novel nine-carbon sugar, pseudaminic acid (Pse),[2] or 5,7-diacetamido-3,5,7,9-tetradeoxy-L-*glycero*-L-*manno*-nonulosonic acid (4). Single Pse moieties are attached via *O*-linkages to both the FlaA and FlaB monomeric structural proteins, at up to 7 and 10 Ser/Thr residues, respectively. The flagella of *C. jejuni* are similarly decorated but with more complex pseudaminic acids, including ones with acetamidino groups (2, 4, 5). This makes the *H. pylori* system more straightforward for analysis of the Pse pathway, although the biosynthetic genes are distributed around the genome, unlike the clustering within the flagellar glycosylation locus seen in *C. jejuni* (6).

The biosynthetic pathway for Pse has been established in outline, based on 1) characterization of UDP-linked intermediates that accumulate in enzyme knockouts in *C. jejuni* (7), 2) recent characterization of UDP-α-D-GlcNAc-modifying dehydratase/aminotransferase pairs from *H. pylori* and *C. jejuni* (8), 3) the presence of homologs of the biosynthetic genes for the related nine-carbon sugar, sialic acid, in the flagellar locus of *C. jejuni* (9, 10) and within the genome of *H. pylori* (11, 12), and 4) the stereochemistry of Pse as determined by structural analysis (5). The prokaryotic biosynthetic pathway for sialic acid is initiated by the epimerization and hydrolysis of UDP-α-D-GlcNAc to ManNAc by the NeuC enzyme. This is followed by condensation of this product with phosphoenolpyruvate by NeuB to give Neu5Ac, which is then activated with CMP by NeuA. In a similar fashion, the biosynthetic pathway of Pse would be initiated by the synthesis of 2,4-diacetamido-2,4,6-trideoxy-β-L-altropyranose from UDP-α-D-GlcNAc. Subsequent steps carried out by enzymes analogous to NeuB and NeuA would then produce the predicted CMP-activated L-*glycero*-L-*manno* conformation of Pse. As is common in the biosynthesis of many complex bacterial deoxyhexoses, *e.g.* in lipopolysaccharide, S-layer, and antibiotic biosynthesis, the GlcNAc conversion is catalyzed by a dehydratase/aminotransferase enzyme pair (13). The dehydratase/epimerase PseB (8) produces the

* This work was supported by the National Research Council's Genomics and Health Initiative and by a grant from the Canadian Institutes of Health Research (Grant 200103GSP-90094-GMX-CFAA-19924 to M. C.). The costs of publication of this article were defrayed in part by the payment of page charges. This article must therefore be hereby marked "*advertisement*" in accordance with 18 U.S.C. Section 1734 solely to indicate this fact.

The atomic coordinates and structure factors (codes 2FN6, 2FNI, and 2FNU) have been deposited in the Protein Data Bank, Research Collaboratory for Structural Bioinformatics, Rutgers University, New Brunswick, NJ (http://www.rcsb.org/).

[1] To whom correspondence should be addressed: Institute for Biological Sciences, National Research Council, 100 Sussex Drive, Ottawa, Ontario K1A 0R6, Canada. Tel.: 613-990-0855; Fax: 613-941-1327; E-mail: Martin.Young@nrc-cnrc.gc.ca.

[2] The abbreviations used are: Pse, 5,7-diacetamido-3,5,7,9-tetradeoxy-L-*glycero*-L-*manno*-nonulosonic acid (also known as pseudaminic acid); AAT, aspartate aminotransferase type I family; AltNAc, *N*-acetyl-β-L-altrosamine; PLP, pyridoxal phosphate; PMP, pyridoxamine phosphate; r.m.s.d., root mean square deviation.

first intermediate in the Pse biosynthetic pathway, UDP-2-acetamido-2,6-dideoxy-β-L-*arabino*-4-hexulose from UDP-α-D-GlcNAc. PseC, an enzyme with predicted aminotransferase activity, was recently shown to perform the next reaction step, the transfer of an amino group in a pyridoxal phosphate (PLP)-dependent manner to form UDP-4-amino-4,6-dideoxy-β-L-AltNAc (8)

The PseC class of enzymes share sequence similarity to PLP-dependent enzymes, which constitute a group of biocatalysts involved in diverse reactions ranging from interconversion of α-amino acids to biosynthesis of amino acids and antibiotic compounds (14, 15). To date, two structures of nucleotide-sugar modifying aminotransferases have been determined: ArnB ((16) PDB entry 1MDX) and PglE (Cj1121c, deposited as PDB entry 1O62). However, neither of these structures was determined as complexes with their respective sugar substrates or products. ArnB synthesizes UDP-4-amino-4-deoxy-β-L-arabinose, found in the modified lipid A of polymyxin-resistant mutants of *Escherichia coli* (17). PglE has recently been identified as the enzyme responsible for aminotransfer during the biosynthesis of UDP-2,4-diacetamido-2,4,6-trideoxy-α-D-glucopyranose in *C. jejuni* (8).

Here we report the crystal structure of PseC (HP0366) from *H. pylori* and its complexes with PLP alone as well as the external aldimine of PLP and the reaction product, UDP-4-amino-4,6-dideoxy-β-L-AltNAc. In addition, we identify residues important in the stabilization of this external aldimine intermediate and determine the stereochemistry of the ligand bound in the PseC active site. Further, we verify the role of PseC in flagellar glycosylation and assembly.

EXPERIMENTAL PROCEDURES

H. pylori Strains and Culture Conditions—*H. pylori* 26695 (11) used for the initial cloning was obtained from R. A. Alm, Astra Zeneca International Boston, *H. pylori* 1061 from Dr. P. Hoffman, Dalhousie University, and M6 from Dr. K. Eaton, Ohio State University, Ohio. Helicobacter strains were grown at 37 °C on antibiotic supplemented trypticase soy agar plates containing 7% (v/v) horse blood in a microaerophillic environment for 48 h.

Construction of pseC Isogenic Mutants—The *pseC* gene HP0366 was amplified by PCR from genomic DNA of strain 26695. The purified product was ligated into pUC19 and confirmed by DNA sequencing. An insertionally inactivated copy of the gene was constructed (pAA0366Kan) according to the method described by Logan *et al.* (18). Isogenic mutants of *H. pylori* strains 1061 and M6 were made by natural transformation as previously described by Haas *et al.* (19). Plasmid pAA0366Kan was used in transformation experiments, and the successful inactivation of the chromosomal copy of the *pseC* gene was confirmed by PCR. Helicobacter cells were tested for motility by spotting cultures onto plates of *Brucella* medium with 0.4% agar and 10% (v/v) fetal bovine serum, or the same medium containing 10 mg/ml kanamycin, with or without 4 mg/ml chloramphenicol.

Construction of the PseC H180N and K183R Substitution Derivatives—Site-directed mutagenesis was performed using the QuikChange mutagenesis kit (Stratagene) according to the manufacturer's instructions with pNRC37 (8) as template. For the K183R mutant we used primers 5′-CGTGTTTAGTTTCCATGCCATTA**G**GCCCATCACTACGGCTGAAGGG-3′ and 5′-CCCTTCAGCCGTAGTGATGGGC**C**TAATGGCATGGAAACTAAACACG-3′, whereas for the H180N mutant we used primers 5′-GCGTTAGCGAGCGTGTTTAGTTTC**A**ATGCCATTAAGCCCATCACTACG-3′ and 5′-CGTAGTGATGGGCTTAATGGCAT**T**GAAACTAAACACGCTCGCTAACGC-3′. The newly constructed plasmids were sequenced as described previously (8).

H. pylori PseC Purification—For functional characterization, His_6PseC and substitution derivatives were purified according to Schoenhofen *et al.* (8) from the expression strain BL21[DE3] (Novagen, Madison, WI) containing the plasmid pNRC37 (8) or derivatives. For crystallization, the cells were lysed by sonication, and the eluted purified protein was dialyzed against 50 mM sodium phosphate, pH 6.5, 0.1 M NaCl, 5% (v/v) glycerol, and 5 mM dithiothreitol overnight at 4 °C. Enzyme purity was assessed by SDS- and native-PAGE and by dynamic light scattering using a DynaPro plate reader molecular sizing instrument (Proterion Corp., Piscataway, NJ) and Dynamics V6 software.

Kinetic Measurements—The dehydratase/epimerase PseB, from *C. jejuni*, was used to prepare the PseC UDP-2-acetamido-2,6-dideoxy-β-L-*arabino*-4-hexulose substrate as previously reported (8). For kinetic analyses, 5 μg of *H. pylori* His_6PseC was incubated at 37 °C in 0.2 ml of 25 mM sodium phosphate, pH 7.2, 50 mM NaCl, containing 1 mM PLP, 10 mM glutamate, and various quantities of UDP-2-acetamido-2,6-dideoxy-β-L-*arabino*-4-hexulose. For the analysis of PseC substitution derivatives, 2 ml of coupled reactions were assembled containing 1 mM UDP-α-D-GlcNAc, 1 mM PLP, 10 mM glutamate, 300 μg of *H. pylori* $PseBHis_6$, and 300 μg of either *H. pylori* His_6PseC-WT, His_6PseC-H180N, or His_6PseC-K183R. Reactions were performed in 25 mM sodium phosphate, pH 7.2, 50 mM NaCl at 37 °C for 3.5 h. Analysis of reaction products by capillary electrophoresis was performed similarly to that by Schoenhofen *et al.* (8). Substrate concentration was determined using the molar extinction coefficient of UDP (ϵ_{260} = 10,000 $liter^{-1}M^{-1}$), and kinetic constants were calculated using Eadie-Hofstee plots with the program GraphPad Prism 3.

Crystallization—PseC was concentrated to 4.5 mg/ml in dialysis buffer, with the addition of 50 mM non-detergent sulfobetaine 221 (Calbiochem). A crystal of apo-PseC was obtained in 2 days at 20 °C from a hanging drop by mixing 1.5 μl of protein in buffer with 1.5 μl of reservoir solution containing 0.2 M ammonium acetate, 0.1 M trisodium citrate, pH 5.6, 30% polyethylene glycol 4000. The crystals belong to space group $P2_12_12$ with unit cell dimensions $a = 87.7$, $b = 155.4$, and $c = 71.5$ Å and $Z = 4$. To obtain the complex with PLP, protein (5 mg/ml) in buffer (20 mM citrate, pH 5.4, 0.1 M NaCl, 5% (v/v) glycerol, and 10 mM dithiothreitol) was incubated with 0.5 mM PLP prior to the crystallization setup. Crystals of the PseC-PLP complex were grown at 20 °C from a hanging drop containing 1.5 μl of protein and 1.5 μl of reservoir solution (21% polyethylene glycol 3350, 0.21 M sodium formate) by vapor diffusion against reservoir solution. Crystals of the PseC-PLP complex belong also to the $P2_12_12$ space group with unit cell dimensions $a = 87.4$, $b = 153.3$, and $c = 70.7$ Å, respectively. The PseC-product complex was prepared by dissolving 0.8 mg of PseC product in 60 μl of protein (5.1 mg/ml) in buffer (20 mM Tris-Cl, pH 8, 100 mM NaCl, 50 mM non-detergent sulfobetaine 201, 10 mM dithiothreitol). The PseC product sample was prepared as previously reported (8) and contained UDP-4-amino-4,6-dideoxy-β-L-AltNAc and UDP-α-D-GlcNAc in the ratio of 85:15, as well as small amounts of PLP and glutamate. Crystals of this complex were obtained by vapor diffusion by mixing 1.5 μl of PseC-product with 1.5 μl of reservoir solution (0.1 M Hepes, pH 7.5, 25% polyethylene glycol 3350) and suspending the drop over a reservoir solution. These crystals belong to the space group $P2_12_12$, with $a = 87.6$, $b = 145.7$, and $c = 66.0$ Å.

Data Collection and Structure Determination—Diffraction data were collected at the National Synchrotron Light Source, Brookhaven National Laboratory at beamline X26, using a Quantum-4 charge-coupled device detector (apo-PseC), or beamline X29, using a Q-315 detector (PseC-product), or with a HTC imaging plate detector mounted on a Rigaku RA-MicroMax 007 generator (Molecular Structure Corp., The

TABLE 1
X-ray crystallographic data

Dataset	Apo	PLP	External aldimine
Data collection			
Unit Cell			
a (Å)	87.7	87.4	87.6
b (Å)	155.4	153.3	145.7
c (Å)	71.5	70.7	65.9
Z	8	8	8
Resolution (Å)	50–2.5	50–3.0	50–1.5
Wavelength (Å)	1.1	1.54	1.1
Observed *hkl*	164,268	92,734	650,567
Unique *hkl*	35,038	18,632	122,065
Redundancy	4.7	5.0	5.4
Completeness	98.9	95.1	89.9 (48)
R_{sym} (%)[a]	0.075	0.098	0.053
$I/\sigma(I)$	40.0	7.1	25.3
Refinement			
Resolution (Å)	50–2.5	50–3.0	50–1.5
R_{work} (*hkl*)[b]	0.215 (33,236)	0.193 (18,470)[c]	0.158 (115,867)
R_{free} (*hkl*)	0.283 (1,754)	0.250 (996)	0.182 (6,144)
B-factor (Å^2), no. of atoms			
Protein	48.7 (5,882)	39.6 (5,921)	12.7 (5,922)
Solvent	44 (112)	26.7 (21)	25.2 (839
Ligands		38.2 (30, PLP)	9.0 (32, PLP), 27.7 (74, sugar)
Ramachandran plot			
Favored (%)	88.6	88.5	90.2
Allowed (%)	10.9	11.2	9.5
Disallowed (%)	0.4	0.3	0.3
r.m.s. deviations			
Bonds (Å)	0.017	0.009	0.010
Angles (°)	1.85	1.08	1.28
PDB code	2FN6	2FNI	2FNU

[a] $R_{sym} = (\Sigma I_{obs} - I_{avg})/\Sigma I_{avg}$.
[b] $R_{work} = (\Sigma F_{obs} - F_{calc})/\Sigma F_{obs}$.
[c] Translation, libration and screw-rotation displacements of a pseudo-rigid body (TLS) correction applied, non-crystallographic restraints applied.

Woodlands, TX) (PseC-PLP). X-ray diffraction data were processed using HKL2000 (20). The apo-PseC structure (2.5-Å resolution) was solved by molecular replacement with the program MOLREP (21) from the CCP4i package (22), using the coordinates of ArnB (PDB 1MDO) as the search model. Refinement of the model was performed using the program REFMAC (23), with no sigma cutoff used in the refinement. The structure of PseC complexed with PLP (3-Å resolution) was solved using the refined native structure as a model. The PLP in the form of internal aldimine was clear in the initial difference electron density map and was included in the refinement. Finally, the structure of PseC co-crystallized with PLP and its product, UDP-4-amino-4,6-dideoxy-β-L-AltNAc was refined to 1.5-Å resolution starting again with the refined native structure as the initial model. The difference electron density showed very clear density for PLP and density for the product but at lower contour levels than for PLP. The density indicated that UDP-4-amino-4,6-dideoxy-β-L-AltNAc forms a covalent bond with PLP yielding an external aldimine. The density for the C5′ and C6′ atoms of the altrose ring was weaker than the density for the rest of the molecule. Data collection and refinement statistics are given in Table 1. Coordinates and structure factors have been deposited with the Protein Data Bank (24) with accession codes 2FN6 (apo-PseC), 2FNI (PseC-PLP), and 2FNU (PseC-product). Topologically related proteins of the PLP-dependent family were investigated with the program VAST (www.ncbi.nlm.nih.gov/Structure/VAST/vast.shtml) and with the SCOP database (25). The conformation of the sugar rings was determined by inputting their coordinates into the six-ring program (www.sao.nrc.ca/ibs/6ring.html) (26).

RESULTS

Phenotypic Characterization of a pseC Mutant—To confirm that *pseC* was involved in flagellar glycosylation, isogenic mutants were generated in two *H. pylori* strains by insertional inactivation. The mutant strains grew well and were not affected in viability or growth characteristics. The motility of *H. pylori pseC* isogenic mutant in strains 1061 (Fig. 1) and M6 (data not shown) was determined by swarming on soft agar plates. When the gene was insertionally inactivated, cells were completely non-motile as demonstrated by the small, sharply delineated colonies typical of non-motile cells on motility agar (Fig. 1*B*). In contrast, the parental strains produced the diffuse spreading growth pattern characteristic of motile bacteria (Fig. 1*A*). Complementation of a *H. pylori* 1061 *pseC* isogenic mutant with the pHel shuttle vector (27) containing the active *pseC* gene restored motility (Fig. 1*C*).

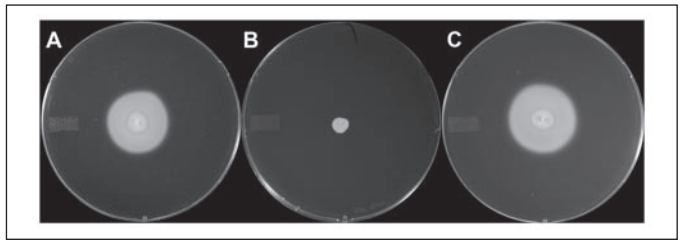

FIGURE 1. **Motility assay of *pseC* mutants.** Motility of *H. pylori* 1061 (*A*) parent strain, the isogenic mutant *H. pylori* 1061 *pseC* (*B*) and its complemented strain, *H. pylori* 1061 *pseC* pHel (*pseC*) (*C*), on motility agar.

Enzyme Characterization—Kinetic analyses of *H. pylori* PseC with the substrate UDP-2-acetamido-2,6-dideoxy-β-L-*arabino*-4-hexulose gave Eadie-Hofstee values of K_m(app) = 0.20 ± 0.029 mM and $k_{cat(app)}$ = 43 ± 3.9 min^{-1}. These values are similar to that reported for the *C. jejuni* PseC homolog (8). The addition of the metal chelators EDTA and EGTA at 5 mM and 1 mM final concentrations, respectively, had no effect on enzyme activity. The *H. pylori* PseC substitution derivatives H180N and K183R exhibited ~66 and 12% β-L-*arabino*-aminotransfer activity, respectively, in relation to the wild-type enzyme.

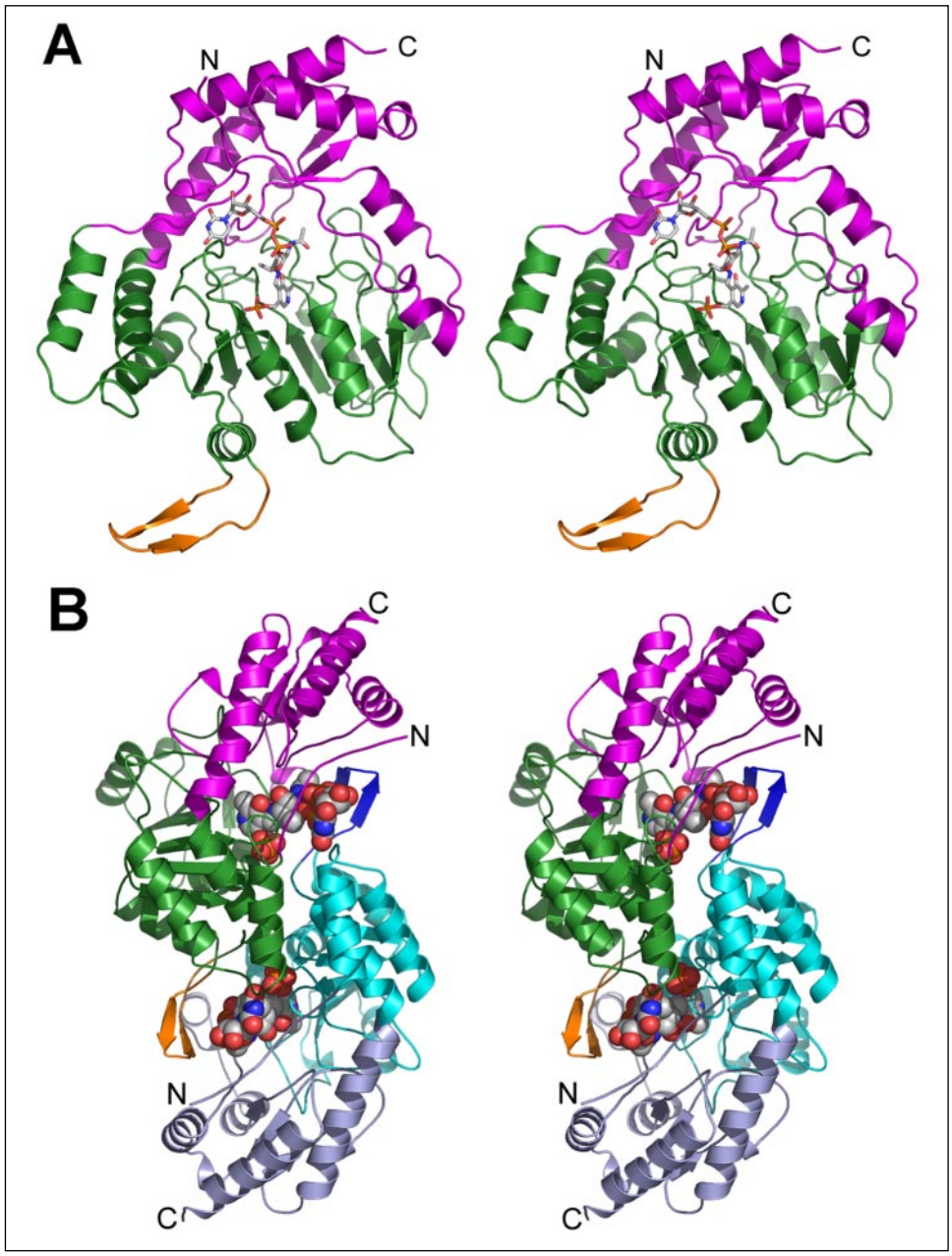

FIGURE 2. **Structure of PseC.** *A*, stereo schematic representation of the monomer with N- and C-terminal domains colored *green* and *magenta*, respectively, and the β-hairpin involved in domain swapping colored *orange; B*, view of the dimer with bound PMP-UDP-L-AltNAc; *C*, the internal aldimine form of PLP in the PseC-PLP complex. The $2F_o - F_c$ electron density map at 3-Å resolution around Lys^{183}-PLP is contoured at the 1 σ level; *D*, $2F_o - F_c$ electron density map at 1.5-Å resolution around the PMP-UDP-L-AltNAc bound to PseC contoured at the 1 σ level.

Monomer and Dimer Structure—Each monomer of PseC can be viewed as made of two α/β/α domains (Fig. 2). The N-terminal domain contains residues Ala^{13}–Lys^{245} and its primary feature is a central, mainly parallel β-sheet having the strand order ↑β1-↓β9-↑β8-↑β5-↑β4-↑β2-↑β3, with strand β9 antiparallel to the rest, flanked on either face by several α-helices. The loop between strands β5 and β8 contains a short two-stranded β-hairpin. Following strand β9 an extended segment of the polypeptide chain consisting of a β-hairpin (residues Gly^{211}–Ile^{225}) juts away from the monomer, and forms domain-swapping type interactions with the other monomer of the dimer. The C-terminal domain contains residues Ala^{1}–Asp^{12} and Ala^{246}–Ile^{374}. It is folded into a three-stranded antiparallel β-sheet with three α-helices that cover one side of this sheet, and a hairpin (Val^{314}–Ala^{343}) containing two α-helices that extend away from the C-terminal domain giving it an L shape. The C-terminal domain packs rather tightly against the N-terminal domain with the exposed side of its β-sheet facing the edge of the β-sheet of the N-terminal domain, and the extended α-helical hairpin laying along the β3 strand on the edge of the N-terminal domain β-sheet (Fig. 2).

PseC is a homodimer in solution (as shown by dynamic light scattering) as well as in the crystal structure, where the two monomers are related by 2-fold crystallographic symmetry (Fig. 2*B*). Upon dimer formation, 2910 $Å^2$ of the solvent-accessible surface of each monomer becomes buried, corresponding to 16.4% of the total surface area of a monomer. Two large and deep cavities are formed at the dimer interface and are the locations of the two active sites. Both subunits are therefore involved in forming the two active sites of the dimer, which are separated by ~30 Å.

The inter-subunit interactions are extensive, involving several elements of secondary structure, predominantly from the N-terminal domains of both monomers. Helix α1 lines up and packs against α1 from the other subunit. The loop following α1 protrudes into the neighboring subunit, forming interactions with the loop regions of that subunit. Helix α3, which covers the central β-sheet, interacts with helix α4 of the large domain of the other subunit. The remaining interface con-

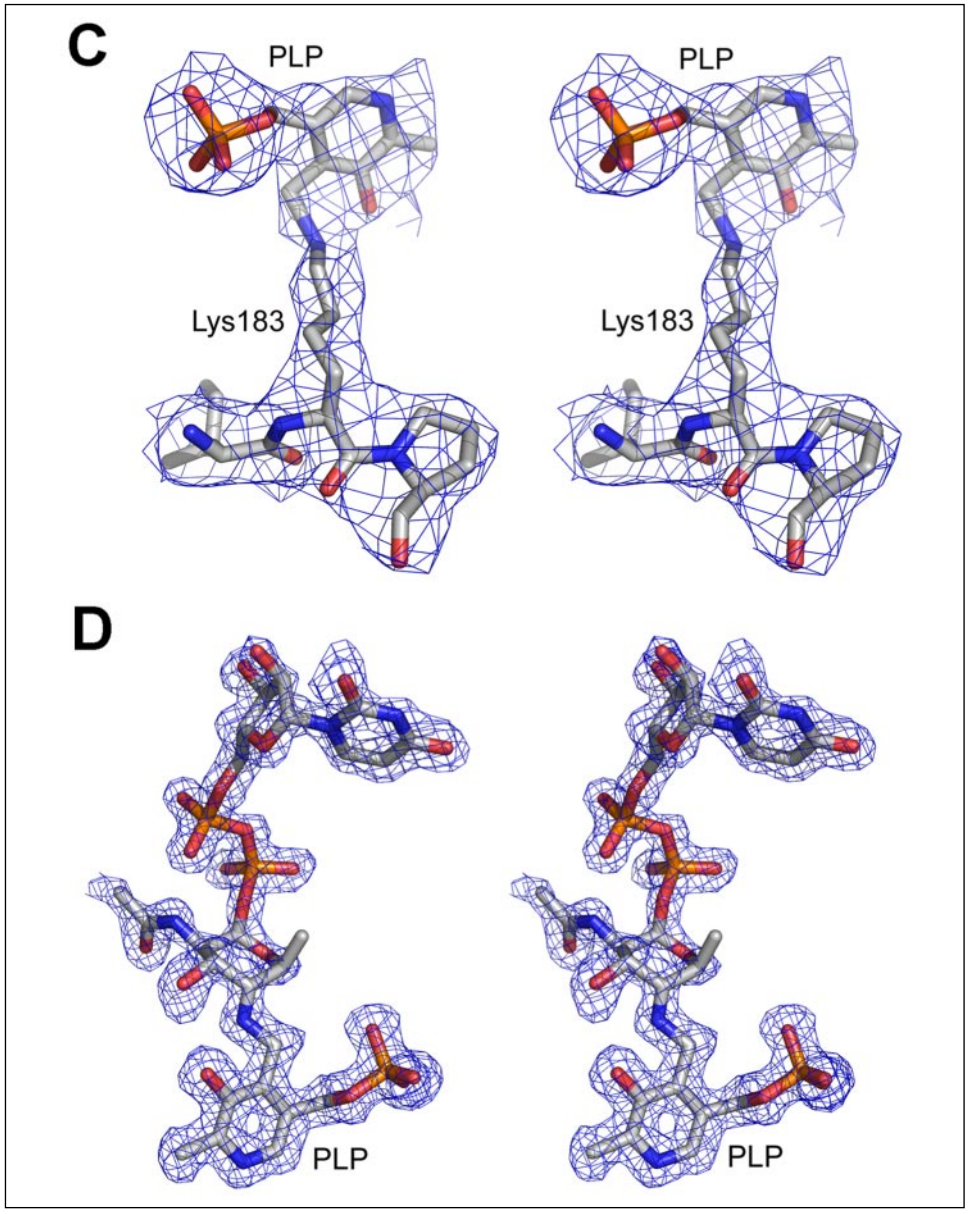

FIGURE 2—*continued*

sists of three α-helices and their loops, which interact with the other subunit. The various interactions at the dimer interface are stabilized by ~30 hydrogen bonds, 10 salt bridges, and many hydrophobic interactions.

Comparison of apo-PseC with the PLP and external aldimine (PMP-UDP-L-AltNAc) complexes shows that the binding of the cofactor and/or product does not invoke any significant conformational changes in the protein, the only difference being in the conformation of Lys^{183}. Small conformational changes occur in the β-hairpin loop of the N-terminal domain (residues Gly^{211}–Ile^{225}) where Lys^{214} is solvent-exposed in the native structure but faces toward the active site cavity in the complexes. This rearrangement also affects to a small extent a few neighboring residues.

The PLP Binding Site—Crystals of PseC obtained in the presence of PLP clearly showed electron density for the PLP cofactor covalently bound to the active site Lys^{183} in the form of an internal aldimine using data collected to 3-Å resolution (Fig. 2*C*). The PLP-binding site is located at a deep cavity formed between the C-terminal ends of the middle strands of the central seven-stranded β-sheet and the N-terminal ends of helices α3 and α4. The aromatic ring of PLP is located at the deep end of this cavity, whereas the phosphate group is near the entrance, also contacting residues from the second molecule of the dimer. Both molecules therefore contribute to each PLP-binding site. The active site Lys^{183}, covalently attached to PLP, is located in the loop between β8 and β9. This orientation of the PLP is such that its *si* side faces the central β-sheet.

The oxygen atoms of the phosphate group of PLP interact with the main-chain amides of Ala^{56} and Thr^{57} (from helix α3), and the side chains of Thr^{57} and Ser^{178} of the first monomer, as well as with the side chain of Asn^{228} and, through a bridging water, with the side chains of His^{210} and Arg^{230} from the second monomer. This phosphate group is located above the N terminus of helix α3, whose dipole moment helps to neutralize the negative charge on the phosphate group.

The pyridine ring of PLP is flanked by Ser^{156} on the *si* face and Phe^{84} on the *re* face. Its phenolic hydroxyl group O3 is within hydrogen bonding distance from the Nε2 atom of His^{157}, the Nζ atom of Lys^{183} and the hydroxyl group of Tyr^{316}. The N1 nitrogen of PLP is within hydrogen bonding distance from the Oδ1 atom of Asp^{154}, indicating the proto-

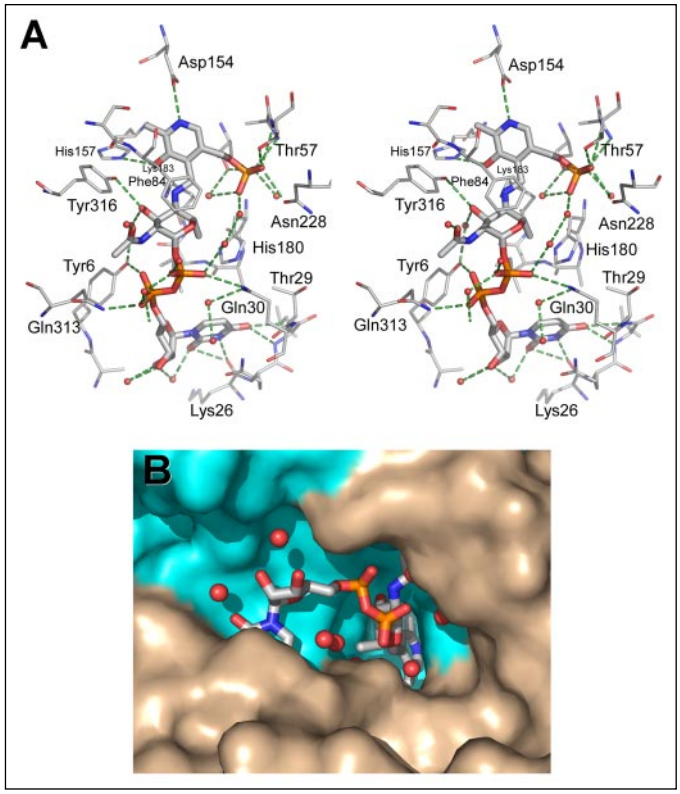

FIGURE 3. **Substrate binding site of PseC with bound PMP-UDP-L-AltNAc.** *A*, stereo view of the substrate binding site in *ball-and-stick* representation. Crucial hydrogen bonds are shown as *dashed lines*; *B*, surface representation with monomers colored in *cyan* and *tan*. The substrate is shown in *ball-and-stick* representation, and water molecules in the binding site are shown as *red spheres*. The PLP moiety is at the *bottom* of the *cleft*.

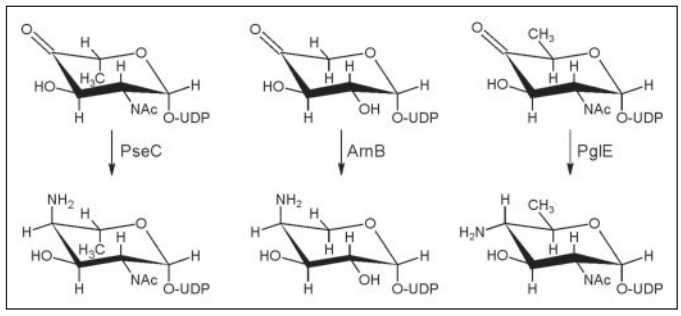

FIGURE 4. **PseC, ArnB, and PglE enzymatic functions.** The substrates of PseC, ArnB, and PglE are UDP-2-acetamido-2,6-dideoxy-β-L-*arabino*-4-hexulose, UDP-β-L-*threo*-pentapyranosyl-4-ulose, and UDP-2-acetamido-2,6-dideoxy-α-D-*xylo*-4-hexulose, respectively. The products of these three enzymes are UDP-4-amino-4,6-dideoxy-β-L-AltNAc, UDP-4-amino-4-deoxy-β-L-arabinose, and UDP-4-amino-4,6-dideoxy-α-D-GlcNAc, respectively. For simplicity, all sugars represented are in the $^4C_1$ configuration.

nated state of the cofactor. The electron sink nature of PLP is enhanced by close interaction of the pyridinium nitrogen with Asp[154], a conserved residue in the aspartate aminotransferase type 1 enzyme family, crucial for maintaining the cofactor in a protonated state (28). Asp[154] is located within strand β5, and its side chain is kept in a proper orientation by hydrogen bonds to Thr[87] and Ser[156].

Substrate Binding Site—Co-crystallization of PseC with the reaction product UDP-4-amino-4,6-dideoxy-β-L-AltNAc and PLP led to a different and much better diffracting crystal form with 8- and 5-Å shorter cell dimensions along the *y*- and *z*-axes, respectively, and a diffraction limit of 1.5 Å. The electron density map of the complex shows density corresponding to PLP and UDP-4-amino-4,6-dideoxy-β-L-AltNAc in each of the two active sites of the PseC dimer and clearly indicates the presence of a covalent bond between the exocyclic C of the PLP and N4 of the altrose, that is, the external aldimine (Fig. 2*D*). The appearance of this intermediate indicates that under these crystallization conditions the reaction proceeded in reverse, converting the product to this covalent intermediate. The electron density for the UDP-sugar is weaker than that for PLP indicating either a greater thermal motion of this molecule or partial occupancy. Indeed, the average temperature factor ⟨*B*⟩ for protein atoms within a 5-Å distance of PLP or the sugar (650 atoms) is 10.3 Å^2, for the PLP it is 8.9 Å^2, for 31 water molecules in the same vicinity it is 21.5 Å^2, whereas for the sugar it is 27.5 Å^2. In particular, the electron density for the C5′ and C6′ atoms of the altrose had the weakest density of all in the UDP-sugar. A possible explanation for this could be that the altropyranose ring is flexible and is known in solution to adopt multiple conformations, although the major fraction of the UDP-sugar in the active site is in a $^4C_1$ conformation. In solution the 4-amino-4,6-dideoxy-β-L-AltNAc sugar ring is in fast dynamic equilibrium with a relative population of 60% $^1C_4$, 25% $^4C_1$, and 15% $^2S_0$ ring conformations (8).

The UDP-sugar binds within the groove leading to the cavity containing PLP and is stabilized by interactions with residues from both monomers. It contacts four contiguous stretches of the polypeptide chain on one molecule, residues Ala[5]–Pro[9], Phe[84], His[180]–Lys[183], and Gln[313]–Tyr[316], and the region Lys[26]–Gln[30] on the second molecule of the dimer (Fig. 3). Water-mediated hydrogen bonding interactions between the UDP molecule and protein side-chain and main-chain atoms add to the stabilization of the complex.

The altrose ring directly contacts only residues from the N-terminal domain. On one side it stacks against the phenyl ring of Phe[84], and on the other side, it is flanked by His[180] and Ile[182]. The *N*-acetyl group is located in a large side cavity leading toward the protein surface and makes only van der Waals contacts with the protein. As well, several water molecules are present in this cavity. The altrose O3′ atom is hydrogen bonded to the hydroxyl of Tyr[316], O3 of PLP, and through a bridging water molecule, to the side chains of His[284] and Tyr[6]. The presence of few constraints on the AltNAc ring by surrounding residues may facilitate conformational changes of the ring that are essential for aminotransferase activity. Of possible relevance for substrate specificity is the presence of two very well ordered water molecules (low *B*-factors) in the vicinity of the C5 atom. One of them (Wat[769]) is hydrogen-bonded to the PLP phosphate and the side chains of Arg[230] and His[210] and is 3.6 Å from the C5 atom, whereas the other (Wat[770]) is hydrogen-bonded to the ring oxygen atom of the AltNAc, to a diphosphate oxygen, and to the side chain of Arg[230] (Fig. 3).

The diphosphate oxygens form direct hydrogen bonds to the side chains of Tyr[6], Gln[30], and Gln[313] and several additional hydrogen bonds through bridging water molecules. Each of the four terminal oxygen atoms makes from one to three hydrogen bonds.

The uridine nucleotide binds with the uracil base in a pocket formed at the dimer interface and forms hydrogen bonds to the second monomer. Its O4 carbonyl is hydrogen-bonded to the NH groups of Leu[28] and Thr[29] and the N3 is hydrogen-bonded to the carbonyl of Lys[26]. The ribose makes no hydrogen bonds to the protein and interacts only through van der Waals contacts with Ala[5] and Ser[7].

DISCUSSION

While the glycosylation of flagellin from a number of important bacterial pathogens has recently received considerable attention (1, 4, 5, 29–31), the functional and structural characterization of the proteins involved in this process is still in its infancy. Here we present the crystal

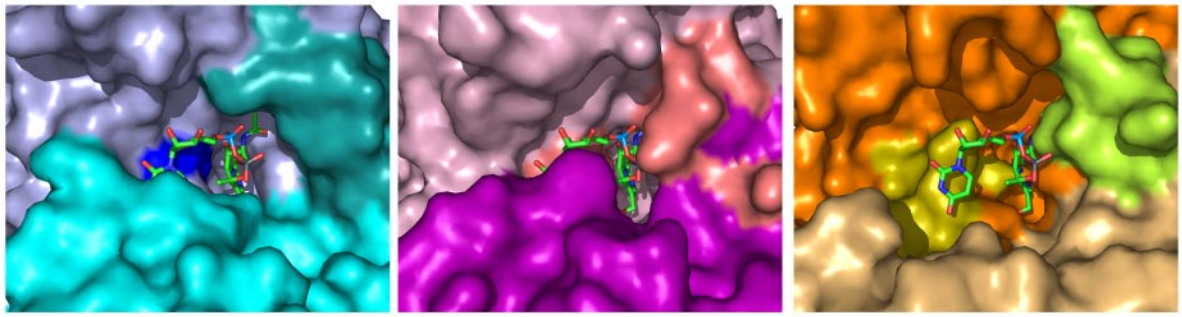

FIGURE 5. **Comparison of the active site regions of PseC (*left*), ArnB (*center*, PDB 1MDO), and PglE (*right*, PDB 1O69).** The molecules were superimposed based on the backbone atoms of the main β-sheet of one molecule of each dimer. The molecules are shown in the same orientation, and the PMP-UDP-L-AltNAc shown in each binding site is taken from PseC. The PLP moiety is at the *bottom* of the *deep cavity*. The two chains in each dimer are shown in *different colors* (PseC: *light blue* and *cyan*; ArnB: *light pink* and *purple*; and PglE: *orange* and *tan*). Two loops are *color-coded*, one to which the UDP moiety binds (on the *left*: in PseC, *blue*; in ArnB, *salmon*; and in PglE, *lemon*) was observed in two different conformations in PglE, and the other limiting the binding site on the *right* (ArnB, *dark salmon*, and PglE, *olive*) is partially disordered in ArnB. Both loops are well ordered in PseC. The cavity in ArnB is narrower at the base than that in PseC, and the *N*-acetyl group collides with the region around residue 314.

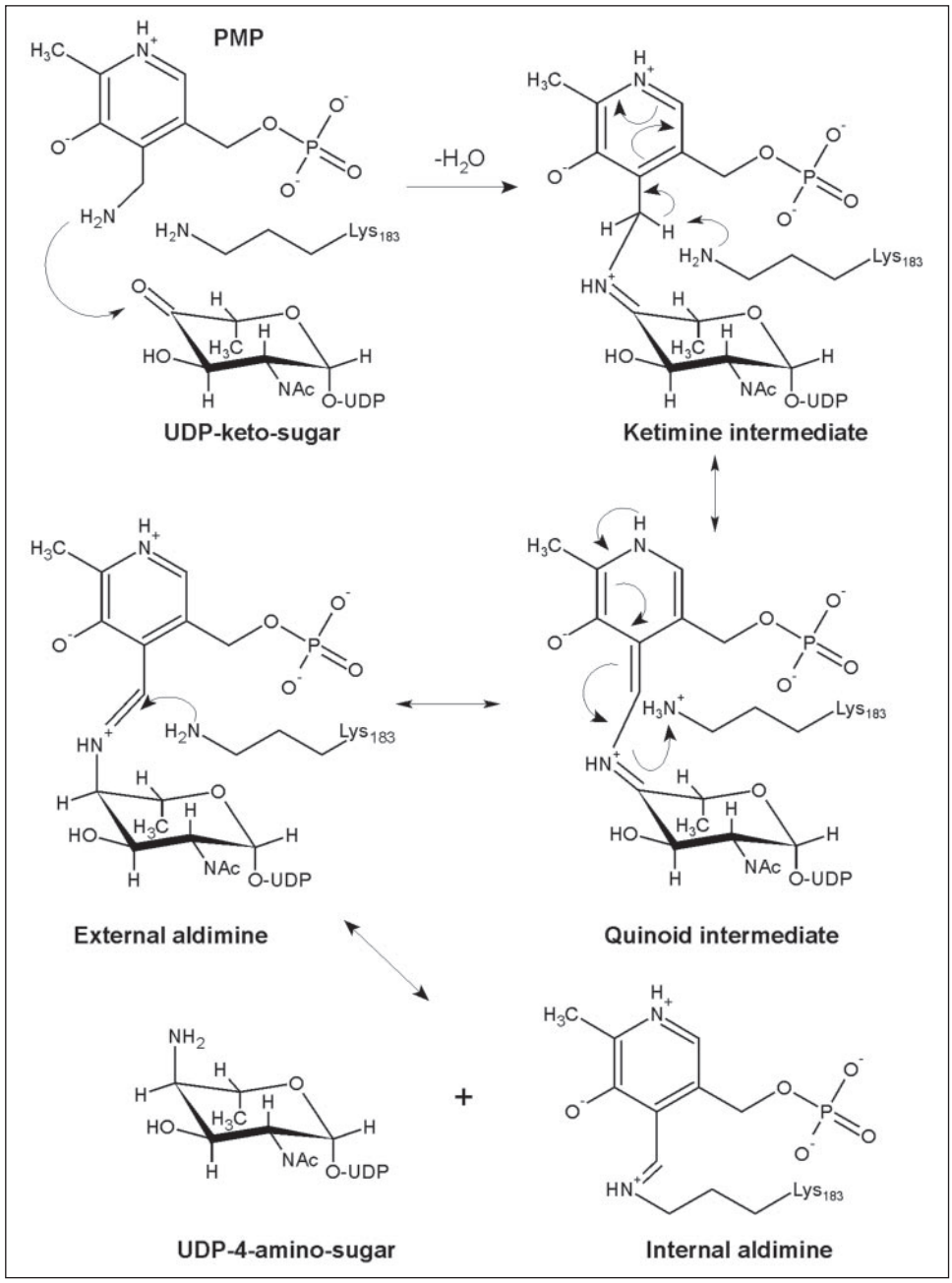

FIGURE 6. **Proposed reaction mechanism for PseC.** The route to the external aldimine, PMP-UDP-L-AltNAc, of Figs. 2*D* and 3 is shown, and its subsequent breakdown to products. Note the sugar stereochemistry observed for the solved external aldimine intermediate is $^4C_1$, in contrast to the predominant $^1C_4$ chair conformation of the UDP-4-amino-sugar product found in solution. For schematic simplicity, all sugars are drawn in the $^4C_1$ form.

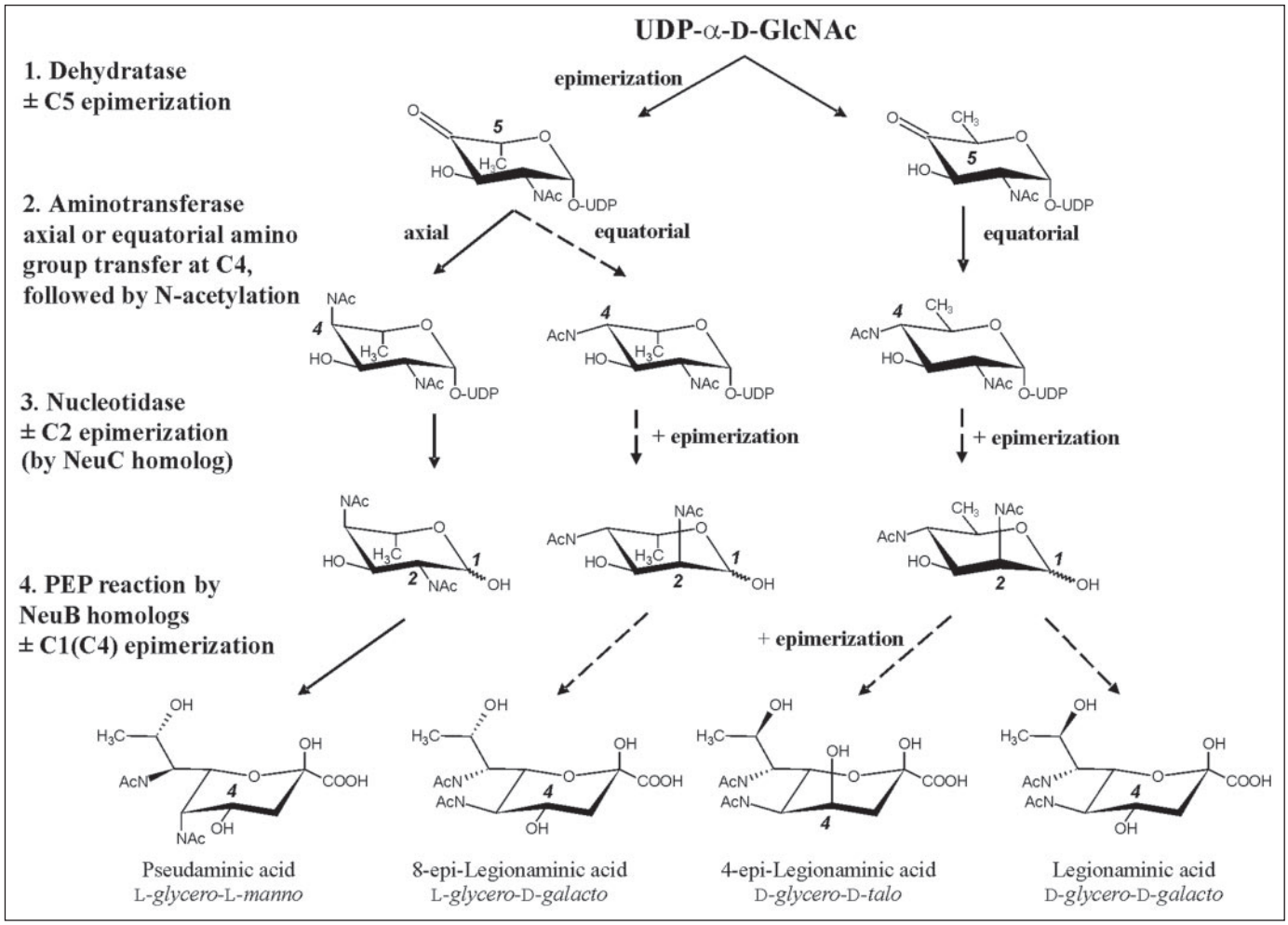

FIGURE 7. **Proposed biosynthetic pathways for Pse and other nonulosonic acids.** *Solid arrows* represent experimentally verified reactions, and *dashed arrows* represent reactions that would be similar to known steps in the Pse or Neu5Ac pathways, with the exception of the last stage of the 4-epilegionaminic acid pathway. The Pse pathway begins with the enzymes PseB and PseC (8), followed at *step 4* by a NeuB homolog (35); the legionaminic acid pathway begins with homologs of *C. jejuni* PglF and PglE (8). All the sugars are shown in $^4C_1$ form except for the nonulosonic acids. The amino groups are assumed to be converted to acetamido groups, though other variants such as acetamidino groups are known. The critical ring positions at which alterations occur in each step are *numbered*.

structure of PseC, a key enzyme involved in the biosynthesis of pseudaminic acid. In particular, the external aldimine complex solved here represents the first structure of a nucleotide-sugar aminotransferase bound with its natural ligand. In addition, we have verified the functional role of PseC in flagellar motility.

The core, mixed seven-stranded β-sheet of PseC classifies the structure within the GABA-aminotransferase-like fold family of PLP-dependent aminotransferases in the SCOP database (25). PseC is most similar in its structure to the ArnB aminotransferase from *Salmonella enterica* serovar Typhimurium (PDB 1MDX, r.m.s.d. 1.2 Å for 330 equivalent Cα atoms, 27% identity), followed by a PLP-dependent enzyme from *C. jejuni* PglE (PDB 1O69, r.m.s.d. 2.1 Å for 342 equivalent Cα atoms, 23.4% identity), and a non-sugar processing enzyme, a 3-amino-5-hydroxybenzoic acid-synthase from *Amycolatopsis mediterranei* (PDB 1B9H, r.m.s.d. 2.3 Å for 365 equivalent Cα atoms, 21.6% identity).

Hwang *et al.* (32) have proposed subdividing the sugar aminotransferases (AAT family VI, or DegT family) into three sub-families, with VI_α having 4-keto-sugar substrates, VI_β having 3-keto-sugar substrates and VI_γ-modifying *scyllo*-inosose. Based on the structural and mechanistic properties of PseC, PglE, and ArnB, plus the nature of their closest homologs in primary sequence, it appears plausible to divide VI_α further. Mechanistically, PseC and ArnB are similar in utilizing L-sugar substrates and adding the amino group axially in the $^4C_1$ ring conformation, whereas PglE uses a D-sugar substrate and attaches the amino group equatorially in the $^4C_1$ ring conformation (Fig. 4). However, PseC and ArnB have distinctly different sets of homologs in GenBank^{TM} (as does PglE), with ArnB having more homologs in *Streptomyces* species, presumably in antibiotic synthesis pathways. Hence the three structures provide useful prototypes for distinct subfamilies of family VI_α.

Comparison of the sugar binding sites of the three enzymes shows they are distinct in the shapes of the binding sites (Fig. 5) and the residues that form them. Some residues, however, are similar among PseC, ArnB, and PglE, including Phe^{84} (Trp and Phe), His^{157} (His and Glu), His^{180} (His and Asn), and Tyr^{316} (Trp and Phe). In a preliminary characterization of binding site residues, His^{180} was changed by site-directed mutagenesis to the Asn found in PglE. Asn does not occur at this position in any of the close homologs of PseC in other organisms, but it is present in approximately half of the homologs of PglE (Tyr and Phe are the most common alternate residues in all these enzymes). The H180N derivative retained its activity and made the same product, indicating this His residue is not a major determinant of PseC substrate specificity.

With a bound sugar being present only in the PseC structure, it is not yet possible to see how the stereochemistry of the incoming amino group is determined, and how the two substrate C5 epimers (Fig. 4) are

differentially recognized by PseC and PglE. However, the structural and substrate similarity of PseC and ArnB (Figs. 4 and 5) allows one to address the question of specificity determinants. The ArnB substrate is a nucleotide keto-sugar, which resembles the substrate of PseC, UDP-2-acetamido-2,6-dideoxy-β-L-*arabino*-4-hexulose. The structure of ArnB was determined only in complex with an inhibitor cycloserine, which forms an external aldimine with PLP (16). The superposition of the two structures shows that the PLP cofactors overlap almost exactly (data not shown). The shape of the substrate binding site is quite similar in both these enzymes, and the UDP portion of the substrate can be easily accommodated in ArnB without any steric clashes, with the uracil making hydrogen bonds to the equivalent backbone NH and carbonyl groups. At first glance, the AltNAc sugar could also fit into the cavity formed near the PLP site in ArnB. However, closer inspection shows that the bottom of the cleft in ArnB around the sugar is narrower than in PseC (Fig. 5) and that a carbonyl group from a residue equivalent to Val^{314} would come very close to the *N*-acetyl group of the AltNAc, which is absent in Ara (Fig. 4), likely resulting in steric hindrance. The cause of this difference may be related to a small difference in orientation and position of the C-terminal domains relative to the N-terminal domains. This could result in a shift of an extended polypeptide segment of ArnB corresponding to residues 310–318 in PseC toward the bound substrate, as well as a different conformation of the 212–222 loop (the latter is partially disordered in ArnB) from the second monomer forming one side of the substrate binding site. Thus, these two enzymes are illuminating examples of fine-tuning of substrate specificity by changes in amino acid sequence that are relatively remote from the active site.

The PLP-binding site residues show much greater conservation than those of the sugar-binding site. The active site lysine (Lys^{183} in PseC) and the aspartate residue close to the pyridine nitrogen of PLP (Asp^{154} in PseC) are absolutely conserved. The serine located near the PLP phosphate (Ser^{178}, interacting with OP3 in PseC) is also fully conserved and occurs five residues before the active site lysine in all the putative aminotransferases. The remaining residues near the active site are semi-conserved within the VI_{α} subfamily, for instance the *re* and *si* side stacking residues Tyr^{316} and Ser^{156} in PseC. The residues near the PLP O3 at the active site are His^{157} in PseC, His^{163} in ArnB, and His^{162} in 3-amino-5-hydroxy benzoic acid synthase, but Glu^{158} is in the equivalent position in PglE. In addition, comparison of PseC, ArnB, and PglE indicates that two loops forming sides of the substrate binding site (181–189 and 212–219 in PseC) are quite mobile and their mobility may play a role in substrate binding and product release. Although both loops are well ordered in PseC, the 181–188 loop assumes two very different conformations in the two molecules of PglE, and the 212–219 loop is partially disordered in ArnB molecules.

The PseC enzyme catalyzes the transfer of an amino group axially at C4 of UDP-2-acetamido-2,6-dideoxy-β-L-*arabino*-4-hexulose (in the $^4C_1$ form), which is a key step in Pse biosynthesis (Fig. 4). This enzyme utilizes a PLP-dependent *trans*-aminase mechanism with glutamate serving as the amino donor. The reaction is similar in nature to that described for ArnB (16). There are two half-reactions; the first is a standard type 1 aminotransferase reaction, which results in an aminated cofactor (PMP). The second half-reaction (Fig. 6) proceeds through the formation of an external aldimine intermediate with the sugar in a $^4C_1$ ring conformation, for which we have determined the detailed structure (Fig. 3). This type of intermediate was proposed for ArnB (16) but has never been proven (33). The C4′ position of this external aldimine intermediate would then undergo a trans-aldimination reaction with Lys^{183} to release the newly aminated sugar-nucleotide. The K183R derivative of PseC, as expected, showed very limited aminotransferase activity. Similar results have also been reported for its homolog in *C. jejuni* (34).

The recent unequivocal characterization of the products of PseB and PseC (8) established that the first steps in the pathway from UDP-α-D-GlcNAc to Pse are as shown in Fig. 7. The next steps would be *N*-acetylation at C4 and removal of the UDP group by a nucleotidase. Epimerization at C2 would not be required for the synthesis of Pse, in contrast to the equivalent NeuC step in the sialic acid pathway. The next step of condensation with phosphoenolpyruvate has been recently confirmed for the *C. jejuni* NeuB homolog Cj1317 (35) and would be followed by addition of CMP by a NeuA homolog. Whereas this route explains the formation of Pse in *H. pylori*, *C. jejuni*, and presumably *P. aeruginosa*, the biosynthesis of additional ald-2-ulosonic acids in other organisms such as *Legionella pneumophila* (36) would require alternate epimerization steps at up to three positions to form the D-*glycero*-D-*galacto* (legionaminic acid) and L-*glycero*-D-*galacto* (8-epilegionaminic acid) structures (Fig. 7).

Legionaminic acid has the same conformation as Neu5Ac, and it could arise from a bacillosamine precursor (*i.e.* 2,4-diacetamido-2,4,6-trideoxy-α-D-Glc), synthesized in the manner of the *C. jejuni* PglF, PglE, and PglD pathway (8) with its dehydratase not carrying out a C5 epimerization and its aminotransferase introducing the amino group equatorially in a $^4C_1$ context (Fig. 7). This putative pathway is supported by the annotation of the gene locus in *L. pneumophila* (37) and the high homology of its aminotransferase LPL0792 to PglE and of its dehydratase LPL0995 to PglF. Epimerization at C2 could then be performed by a NeuC homolog, in the manner of neuraminic acid biosynthesis. 8-Epilegionaminic acid would require similar processes, except for C5 epimerization by the dehydratase in the manner of Pse. Interestingly, the structure of 4-epilegionaminic acid implies that its NeuB homolog adds the three-carbon fragment from phosphoenolpyruvate in the opposite stereochemistry to that of the other three nonulosonic acids. Thus the variation in the nonulosonic acids can arise entirely from alternate stereochemistries during the four synthetic steps, with no additional epimerases being required, and the four products represent only one-quarter of the possible isomers that could be made in this way.

As a result of the adaptive ability of bacteria to develop resistance to current antibiotics, new strategies to target bacterial pathogens are urgently required. One such strategy is to specifically target the key virulence determinants of these pathogens and thus reduce the selection pressure on the total microflora (38, 39). Motility is one such virulence determinant for both *Helicobacter* and *Campylobacter*, enabling the organisms to avoid the natural flow of the gastrointestinal tract and to colonize the gastric and intestinal mucosa (40, 41). As glycosylation is essential for flagella assembly in both organisms (3, 4), and hence motility, the Pse biosynthetic pathway has potential for therapeutic targets, and PseC provides an optimal target within this pathway on several grounds. It appears to act before the elaboration of the Pse precursor into multiple forms, it has no homolog in the human Neu5Ac pathway, and inhibitors of it may also disrupt the biosynthesis of the related ald-2-ulosonic acids that occur in the lipopolysaccharides of a number of significant pathogens (36).

Acknowledgments—X-ray diffraction data for this study were measured at beamlines X8C, X26, and X29 of the National Synchrotron Light Source. We thank Martin McMillan and Leonid Flaks (beamline X8C) and Howard Robinson (beamline X29) for assistance in data collection. Financial support comes principally from the Office of Biological and Environmental Research and of Basic Energy Sciences of the U.S. Department of Energy, and the National Center for Research Resources of the National Institutes of Health. We also thank Chuong Huynh for his technical assistance in the preparation of the site-directed mutants, Simon Foote for bioinformatics assistance, and Drs. Dennis Whitfield and Evgeny Vinogradov for helpful discussions.

REFERENCES

1. Arora, S. K., Neely, A. N., Blair, B., Lory, S., and Ramphal, R. (2005) *Infect. Immun.* **73,** 4395–4398
2. Logan, S. M., Kelly, J. F., Thibault, P., Ewing, C. P., and Guerry, P. (2002) *Mol. Microbiol.* **46,** 587–597
3. Goon, S., Kelly, J. F., Logan, S. M., Ewing, C. P., and Guerry, P. (2003) *Mol. Microbiol.* **50,** 659–671
4. Schirm, M., Soo, E. C., Aubry, A. J., Austin, J., Thibault, P., and Logan, S. M. (2003) *Mol. Microbiol.* **48,** 1579–1592
5. Thibault, P., Logan, S. M., Kelly, J. F., Brisson, J. R., Ewing, C. P., Trust, T. J., and Guerry, P. (2001) *J. Biol. Chem.* **276,** 34862–34870
6. Szymanski, C. M., Logan, S. M., Linton, D., and Wren, B. W. (2003) *Trends Microbiol.* **11,** 233–238
7. Soo, E. C., Aubry, A. J., Logan, S. M., Guerry, P., Kelly, J. F., Young, N. M., and Thibault, P. (2004) *Anal. Chem.* **76,** 619–626
8. Schoenhofen, I. C., McNally, D. J., Vinogradov, E., Whitfield, D., Young, M., Dick, S., Wakarchuk, W. W., Brisson, J.-R., and Logan, S. M. (2006) *J. Biol. Chem.*, **281,** 723–732
9. Guerry, P., Doig, P., Alm, R. A., Burr, D. H., Kinsella, N., and Trust, T. J. (1996) *Mol. Microbiol.* **19,** 369–378
10. Parkhill, J., Wren, B. W., Mungall, K., Ketley, J. M., Churcher, C., Basham, D., Chillingworth, T., Davies, R. M., Feltwell, T., Holroyd, S., Jagels, K., Karlyshev, A. V., Moule, S., Pallen, M. J., Penn, C. W., Quail, M. A., Rajandream, M. A., Rutherford, K. M., van Vliet, A. H., Whitehead, S., and Barrell, B. G. (2000) *Nature* **403,** 665–668
11. Tomb, J. F., White, O., Kerlavage, A. R., Clayton, R. A., Sutton, G. G., Fleischmann, R. D., Ketchum, K. A., Klenk, H. P., Gill, S., Dougherty, B. A., Nelson, K., Quackenbush, J., Zhou, L., Kirkness, E. F., Peterson, S., Loftus, B., Richardson, D., Dodson, R., Khalak, H. G., Glodek, A., McKenney, K., Fitzegerald, L. M., Lee, N., Adams, M. D., and Venter, J. C. (1997) *Nature* **388,** 539–547
12. Alm, R. A., Ling, L. S., Moir, D. T., King, B. L., Brown, E. D., Doig, P. C., Smith, D. R., Noonan, B., Guild, B. C., deJonge, B. L., Carmel, G., Tummino, P. J., Caruso, A., Uria-Nickelsen, M., Mills, D. M., Ives, C., Gibson, R., Merberg, D., Mills, S. D., Jiang, Q., Taylor, D. E., Vovis, G. F., and Trust, T. J. (1999) *Nature* **397,** 176–180
13. Trefzer, A., Salas, J. A., and Bechthold, A. (1999) *Nat. Prod. Rep.* **16,** 283–299
14. Mehta, P. K., and Christen, P. (1998) *Adv. Enzymol. Related Areas of Mol. Biol.* **74,** 129–184
15. Jansonius, J. N. (1996) *Curr. Opin. Struct. Biol.* **8,** 759–769
16. Noland, B. W., Newman, J. M., Hendle, J., Badger, J., Christopher, J. A., Tresser, J., Buchanan, M. D., Wright, T. A., Rutter, M. E., Sanderson, W. E., Muller-Dieckmann, H. J., Gajiwala, K. S., and Buchanan, S. G. (2002) *Structure* (*Camb.*) **10,** 1569–1580
17. Breazeale, S. D., Ribeiro, A. A., and Raetz, C. R. (2003) *J. Biol. Chem.* **278,** 24731–24739
18. Logan, S. M., Conlan, J. W., Monteiro, M. A., Wakarchuk, W. W., and Altman, E. (2000) *Mol. Microbiol.* **35,** 1156–1167
19. Haas, R., Meyer, T. F., and van Putten, J. P. (1993) *Mol. Microbiol.* **8,** 753–760
20. Otwinowski, Z., and Minor, W. (1997) *Methods Enzymol.* **276,** 307–326
21. Vagin, A. A., and Isupov, M. N. (2001) *Acta Crystallogr. D. Biol. Crystallogr.* **57,** 1451–1456
22. Potterton, E., Briggs, P., Turkenburg, M., and Dodson, E. (2003) *Acta Crystallogr. D. Biol. Crystallogr.* **59,** 1131–1137
23. Murshudov, G. N., Vagin, A. A., Lebedev, A., Wilson, K. S., and Dodson, E. J. (1999) *Acta Crystallogr. D. Biol. Crystallogr.* **55,** 247–255
24. Berman, H. M., Bhat, T. N., Bourne, P. E., Feng, Z., Gilliland, G., Weissig, H., and Westbrook, J. (2000) *Nat. Struct. Biol.* **7,** (suppl.) 957–959
25. Murzin, A. G., Brenner, S. E., Hubbard, T., and Chothia, C. (1995) *J. Mol. Biol.* **247,** 536–540
26. Berces, A., Whitfield, D. M., and Nukada, T. (2001) *Tetrahedron* **57,** 477–491
27. Heuermann, D., and Haas, R. (1998) *Mol. Gen. Genet.* **257,** 519–528
28. John, R. A. (1995) *Biochim. Biophys. Acta* **1248,** 81–96
29. Schirm, M., Arora, S. K., Verma, A., Vinogradov, E., Thibault, P., Ramphal, R., and Logan, S. M. (2004) *J. Bacteriol.* **186,** 2523–2531
30. Schirm, M., Kalmokoff, M., Aubry, A., Thibault, P., Sandoz, M., and Logan, S. M. (2004) *J. Bacteriol.* **186,** 6721–6727
31. Arora, S. K., Bangera, M., Lory, S., and Ramphal, R. (2001) *Proc. Natl. Acad. Sci. U. S. A.* **98,** 9342–9347
32. Hwang, B. Y., Lee, H. J., Yang, Y. H., Joo, H. S., and Kim, B. G. (2004) *Chem. Biol.* **11,** 915–925
33. Field, R. A., and Naismith, J. H. (2003) *Biochemistry* **42,** 7637–7647
34. Obhi, R. K., and Creuzenet, C. (2005) *J. Biol. Chem.* **280,** 20902–20908
35. Chou, W. K., Dick, S., Wakarchuk, W. W., and Tanner, M. E. (2005) *J. Biol. Chem.* **43,** 35922–35928
36. Knirel, Y. A., Shashkov, A. S., Tsvetkov, Y. E., Jansson, P. E., and Zahringer, U. (2003) *Adv. Carbohydr. Chem. Biochem.* **58,** 371–417
37. Luneberg, E., Zetzmann, N., Alber, D., Knirel, Y. A., Kooistra, O., Zahringer, U., and Frosch, M. (2000) *Int. J. Med. Microbiol.* **290,** 37–49
38. Kauppi, A. M., Nordfelth, R., Uvell, H., Wolf-Watz, H., and Elofsson, M. (2003) *Chem. Biol.* **10,** 241–249
39. Nordfelth, R., Kauppi, A. M., Norberg, H. A., Wolf-Watz, H., and Elofsson, M. (2005) *Infect. Immun.* **73,** 3104–3114
40. Eaton, K. A., Suerbaum, S., Josenhans, C., and Krakowka, S. (1996) *Infect. Immun.* **64,** 2445–2448
41. Black, R. E., Levine, M. M., Clements, M. L., Hughes, T. P., and Blaser, M. J. (1988) *J. Infect. Dis.* **157,** 472–479

Structural and Functional Characterization of PseC, an Aminotransferase Involved in the Biosynthesis of Pseudaminic Acid, an Essential Flagellar Modification in *Helicobacter pylori*

Ian C. Schoenhofen, Vladimir V. Lunin, Jean-Philippe Julien, Yunge Li, Eunice Ajamian, Allan Matte, Miroslaw Cygler, Jean-Robert Brisson, Annie Aubry, Susan M. Logan, Smita Bhatia, Warren W. Wakarchuk and N. Martin Young

J. Biol. Chem. 2006, 281:8907-8916.
doi: 10.1074/jbc.M512987200 originally published online January 18, 2006
